Field and Laboratory Evaluations of Commercial and Next Generation Alumina-Forming Austenitic Foil for Advanced Recuperators

Bruce A. Pint, Sebastien Dryepondt, Michael P. Brady,
Yukinori Yamamoto, Bo Ruan* and Robert D. McKeirnan, Jr.*
Oak Ridge National Laboratory, Materials Science and Technology Division
Oak Ridge, TN 37831-6156 Phone: (865) 576-2897, E-mail: pintba@ornl.gov
*Capstone Turbine Corp., Chatsworth, CA Phone: (818) 407-3666, E-mail: rmck@capstone-turbine.com

ABSTRACT

Alumina-forming austenitic (AFA) steels represent a new class of corrosion- and creep-resistant austenitic steels designed to enable higher temperature recuperators. Field trials are in progress for commercially rolled foil with widths over 39 cm. The first trial completed 3,000 h in a microturbine recuperator with an elevated turbine inlet temperature and showed limited degradation. A longer microturbine trial is in progress. A third exposure in a larger turbine has passed 16,000 h. To reduce alloy cost and address foil fabrication issues with the initial AFA composition, several new AFA compositions are being evaluated in creep and laboratory oxidation testing at 650°-800°C and the results compared to commercially fabricated AFA foil and conventional recuperator foil performance.

INTRODUCTION

Combined Heat and Power (CHP) systems are an attractive distributed generation (DG) solution offering high (>80%) efficiency and flexible operation. Waste heat from a small gas turbine can be used for process heat, steam generation and/or heating and cooling [1-4]. Strategies to increase the market penetration of turbine-based CHP systems include decreasing current materials costs and increasing electrical efficiency, while maintaining low emissions. Two key pathways to higher efficiency are recuperation and higher turbine inlet temperatures. Small (<5MW) gas turbines (and especially 25-

400 kW microturbines [5-7]) can significantly increase efficiency (<30% for microturbines, <40% for small gas turbines) by using the turbine exhaust gas to preheat the compressed air in a recuperator [7-10] before it enters the combustor. Increasing the turbine inlet temperature can cause material selection and durability issues in the hot section and the recuperator, typically requiring more expensive materials with higher temperature capability.

High efficiency recuperators typically rely on thin-walled (75-125μm, 3-5 mil) metal foils in order to maximize heat transfer [8-10]. Since the push to higher efficiency DG/CHP systems began ~20 years ago, it is now well-established that conventional stainless steel foils, such as type 347 (Table 1), are rapidly attacked in exhaust gas due to the formation of a volatile oxy-hydroxide ($CrO_2(OH)_2$) when the Cr-rich oxide on the steel surface reacts with water in the exhaust above 600°C [11-18]. Less appreciated is that the same mechanism affects all Cr_2O_3-forming foils, including Ni-base alloy 625. Consumption of the limited Cr reservoir present in a ~100μm thick foil can be dominated by linear volatilization kinetics, rather than the slower, parabolic oxidation kinetics for Cr_2O_3 formation, especially at higher gas velocities and long exposure times (minimum 30-40 kh recuperator lifetime). For current ~650°C recuperator temperatures, turbine manufacturers have turned to alloy 625, Nb-modified Fe-20Cr-25Ni (composition similar to alloy 709) and alloy 120 foils (Table 1) [19-21]. All of these alloys are susceptible to accelerated degradation due to volatilization and significant Cr losses have been quantified in long-term laboratory and field exposures [14-16,18,20-22]. The rate of Cr loss increases with temperature and this has been studied in laboratory testing [14,15,23]. Figure 1 shows that after only 6kh at 800°C, the Cr content in 625 foil has dropped from 23wt.% to <18% due to oxide formation and Cr volatilization. Obviously, if the recuperator needs to operate for 25-40kh [20-22], the rate of Cr loss is unacceptably high at 800°C. Almost 25% of the total alloy Cr reservoir in the foil had been consumed in only 6kh. When the Cr content drops below some critical level (~15%Cr), more accelerated oxidation would be expected as the alloy would no longer be able to exclusively form a protective Cr-rich oxide and more Ni-rich oxide would form. Even after 10kh at 700°C, significant Cr loss was measured, Figure 1. If a similar linear rate persisted for 40kh, the 625 foil would be severely depleted. For the next generation of recuperators to operate at 700°C or higher temperatures, more oxidation resistant alloys are

needed.

In 2007, a new class of Fe-base creep-resistant alumina-forming austenitic (AFA) alloys was developed, relevant to higher temperature recuperator application [24-30]. Alloys that form an Al-rich surface oxide are more resistant to oxidation in the presence of water vapor because of the higher stability of α-Al_2O_3[13]. The AFA alloy properties are well-suited for thin-walled recuperators because of the combination of creep strength, which approaches that of alloy 709, and oxidation resistance not found in the other candidate alloy foils [26-30]. Laboratory testing of AFA foil (composition F4 in Table 1) has shown protective behavior after 10kh at 800°C in wet air (10%H_2O) used to simulate exhaust gas [30] and in initial engine trials using sheet material [28]. Progress continues on commercializing AFA foil for recuperators with an update on laboratory testing of commercial foil [30] and the completion of the first engine test in a rainbow recuperator with alloy 120. In addition, an update is provided on laboratory evaluation of new AFA compositions with lower cost, similar properties and easier processing parameters [30].

EXPERIMENTAL PROCEDURE

Laboratory scale (~13 kg) vacuum induction melted (VIM) heats of AFA compositions were cast by Carpenter Technology Corp. Further details of the laboratory-scale processing were provided previously [27]. For these four new AFA compositions (Table 1), the solutionizing temperature was lowered from 1200°C (used for previous laboratory batches) to 1100°C, resulting in a grain size of 5-10 μm. Their compositions were selected to lower the raw material cost of the alloy relative to the F4 composition, especially by lowering the Nb, W and Ni contents [30]. In addition, larger (1100 and 4500 kg) commercial heats of F4 were produced for commercial processing to foil. The first F4 foil batches were ~18 cm wide and 80 and 106 μm thick (3.2 and 4.2 mil). Subsequent batches were 80 μm (~21 cm wide), 106 μm (~39 cm wide) and 150 μm (15 cm wide) fabricated by two different suppliers. As-fabricated microstructures have been reported previously [30]. Both of the wider foil batches were successfully folded for fabrication into recuperator air cells and the ~80 μm x 21 cm foil was engine tested in a 65 kW microturbine at Capstone Turbine Corp. This turbine has been modified to produce exhaust temperatures

of ~720°C and has been detailed elsewhere [20].

For laboratory testing, creep specimens were machined by electro-discharge machining. The creep specimens were 114 mm (4.5 in.) long with a gauge length of 25.4 mm (1 in.) and 6.35 mm (0.25 in) wide. The shoulders were approximately 16mm wide. Pads of the same thickness as the foil were spot-welded on the shoulders for re-enforcement and 3.17 mm (0.125 in.) diameter pin holes were cut in the shoulders for gripping. The extensometer was a rod-in-tube type that transmitted extension out of the hot zone of the furnace to averaging LVDT sensors. Because of the small section areas, specimens were dead loaded. Creep testing was performed in laboratory air at 650°C with a 250 MPa load, at 677°C with 117 MPa load and at 750°C with 100 MPa load to induce rupture in a reasonably short time.

Foil oxidation coupons (~12 mm x 18 mm x ~80-150 μm) were tested in the as-annealed surface condition and ultrasonically cleaned in acetone and methanol prior to oxidation. Exposures were 100 h cycles at 650°, 700°, 750° or 800°C and mass changes were measured after every cycle using a Mettler-Toledo model XP205 balance, with an accuracy of ±0.04 mg or ±0.01 mg/cm^2. The amount of water injected was used to calibrate the water content at 10±1 vol.% for these experiments. Up to 40 specimens were positioned in alumina boats in the furnace hot zone so as to expose the specimen faces parallel to the flowing (~1.7-1.9 cm/s) gas. After laboratory exposures, specimens were Cu-plated and sectioned for metallographic analysis. A similar metallographic procedure was used for the engine-exposed foil.

RESULTS

Laboratory Testing of Commercial AFA Foils

A brief update is provided of the oxidation and creep data provided earlier [30]. Figure 2 shows polished cross-sections of the first commercial AFA foil batches (with the commercial F4 composition shown in Table 1) that were 80 and 106 μm thick after 10,000 h exposures at 650°-800°C. In general, thin reaction products were observed with occasional oxide nodules formed. A small amount of internal oxidation was observed that may be associated with internal nitridation of the as-annealed foil (due to N_2 in the environment). The depth of internal attack did not change significantly with exposure temperature and was more notable for the 106 μm thick foil, Figure 2.

Figure 3 summarizes the creep results for these commercial AFA foils compared to commercial foil of 347, 310, 120 and 709 (2025Nb). At the two conditions investigated, the time to rupture is shown as well as the time to 5% strain. At 5% strain the recuperator deformation is significant and airflow is restricted. For the accelerated conditions at 750°C, the alloy 709 and 120 times to 5% strain are 50-190% higher than the AFA foils. These alloys also showed an advantage at 677°C, with the alloy 120 specimen rupturing at almost 35,000 h. However, the time to 5% strain for alloy 709 (~9,000 h) at 677°C was comparable to the AFA foils. For oxidation-resistant 310 foil with similar Cr content as alloys 120 and 625, the creep properties are very poor due to a lack of elements such as Nb needed to form stable carbides, Table 1.

Engine Testing of Commercial AFA Foil

Figure 4 shows a completed air cell with AFA foil like those used for the engine test on a 65kW (model C65) microturbine. The recuperator consisted of a mixture of AFA and alloy 120 air cells for a comparison of their relative performance. The engine ran for a total of 3,000 h with an increased recuperator inlet temperature of ~720°C and the engine was cycled 3,000 times to simulate the heating and cooling of much longer applications. During the test, no drop in engine performance was observed. After completion, sections of the recuperator were removed for characterization of both foils, Figure 5. Figures 6 and 7 show polished cross-sections of the foils in the hottest locations of the air cells. Copper plating was used to assist in protecting and imaging the thin reaction products, however, the plating was not uniform. Similar to the laboratory exposures of the F4 foil shown in Figure 2, the scale formed on the F4 air cells after the engine test was generally thin with occasional oxide nodules, Figure 6. In a few convex locations, larger oxide nodules formed with one of the worst locations shown in Figure 6c. The nodules appear to have the duplex structure typical of Fe-rich oxides formed in exhaust gas. Their selective formation in these locations was surprising and further characterization is in progress to determine any potential reason for this observation. Figure 7 shows similar images from alloy 120 foil air cells. As expected, a thin reaction product was observed on both sides of the foil. Figure 7c shows an example of the small oxide nodules that were occasionally observed on this material.

A second rainbow core was assembled for a longer (8kh) C65 microturbine engine test at ORNL that

is in progress and should conclude in late 2016. Based on the occasional nodule formation observed in the 3,000 h test, this longer test will assist in indicating if any oxidation issues exist for the AFA F4 composition in the engine. In addition, folded AFA F4 panels have been exposed in an exhaust duct of a recuperated 4.6 MW turbine since January 2013. This is the same location that specimens of 625 and 2025Nb (709) have been exposed previously [19,21]. The first AFA panel removed from this exposure will have more than 16 kh of exposure time.

Laboratory Testing of New AFA Compositions

Initial oxidation and creep data were reported earlier [30] for the four new laboratory-scale AFA compositions, which were optimized for a final anneal of only 1100°C (rather than 1200°C for the F4 composition) and used lower levels of Nb, W and/or Ni to lower the cost of AFA foil, Table 1. The alloying strategy was discussed previously [30]. Of course, these leaner compositions were not expected to perform as well as the F4 composition. Figure 8 shows the long-term oxidation behavior of these new AFA foils at 700°C in humid air. The AFA foils with only 20%Ni (F20N and F20W) began to show signs of accelerated oxidation after 3-6 kh. In contrast, the 25%Ni AFA foils (F25N and F25W) showed low mass gains for 10 kh, similar to the commercial F4 foil shown for comparison in Figure 8. Figure 9 shows the same foils at 800°C in humid air. At this higher temperature, many of the specimens showed higher mass gains almost immediately, except for the 25%Ni composition with W, F25W, which matched the F4 performance for 10 kh.

The creep testing of these alloys showed a much different performance ranking, Figure 10. The new alloys were first evaluated at 750°C/100MPa to provide a rapid evaluation [30] and several compositions had times to 5% strain similar to F4 foil. The F25W foil, which exhibited the best oxidation resistance, had the lowest creep rupture life at 750°C. This composition was most strongly affected by the lower final annealing temperature (1100°C rather than 1200°C). The F25W composition had the lowest C content (0.1%) of the four alloys, Table 1, and relies on MC supersaturation for 750°C creep strength while the other alloys with 0.2%C form $M_{23}C_6$ [29,31]. Because of the long lifetimes observed at 677°C/117MPa (Figure 3), the new AFA foils were evaluated at 650°C/250MPa. With these conditions, the F20W foil performed exceptionally well and the higher creep rupture lifetime for F20W compared to

F20N, suggests more than just the 1%W addition contributed to the excellent creep behavior. Nevertheless, the poor oxidation behavior of both 20%Ni compositions, Figures 8 and 9, suggests that F25N is the most attractive new AFA composition. Taking into account that the F25N foil had a finer grain size (<10μm) than the 27 μm grain size in the commercial F4 material, the F25N creep behavior is very promising. The F25N composition retained good oxidation resistance at 700°C but not at 800°C. If higher temperature oxidation resistance were needed, higher Al contents in F25N (up to 4%) are a potential variation to investigate.

CONCLUSION

The development of alumina-forming austenitic steels has progressed to the first engine tests of AFA air cells and folded material. The 3,000 h/3,000 cycle engine test resulted in no drop in engine performance during this exposure. A few large oxide nodules were observed on the AFA foil after the engine test and a longer (8,000 h) engine test is in progress. Excellent oxidation behavior of the commercially fabricated AFA F4 foil has been observed in laboratory testing at 650°-800°C, similar to previous laboratory-made sheet and foil specimens. In addition to the current F4 composition, new AFA foil compositions are being evaluated which are expected to have lower cost and easier fabrication with a solutionizing anneal temperature of only 1100°C (rather than 1200°C). Development of a lower-cost AFA grade with similar creep and oxidation properties and easier processing is being pursued in order to increase the possibility for an AFA foil to be commercially adopted for future high-efficiency CHP applications.

ACKNOWLEDGMENTS

The author would like to thank M. Stephens, J. Moser, T. Lowe and T. Jordan at ORNL for assistance with the experimental work, and P. F. Tortorelli for comments on the manuscript. This research was sponsored by the U.S. Department of Energy, Office of Energy Efficiency and Renewable Energy, Advanced Manufacturing Office (Combined Heat and Power).

REFERENCES

1. Maidment, G. G. and Tozer, R. M., 2002 "Combined Cooling Heat and Power in Supermarkets," Applied Thermal Engineering, **22**, pp.653-65.
2. Alanne, K. and Saari, A., 2004 "Sustainable Small-Scale CHP Technologies for Buildings: The Basis for Multi-Perspective Decision-Making," Renewable and Sustainable Energy Reviews, **8**, pp.401-31.
3. Kuhn, V., Klemes, J. and Bulatov, I., 2008 "MicroCHP: Overview of Selected Technologies, Products and Field Test Results," Applied Thermal Engineering **28**, pp.2039–2048.
4. Chicco, G. and Mancarella, P., 2009 "Distributed multi-generation: A comprehensive view," Renewable Sustainable Energy Rev. **13**, pp.535-551.
5. Watts, J. H., 1999, "Microturbines: A New Class of Gas Turbine Engine," Global Gas Turbine News, **39**(1), pp.4-8.
6. Hamilton, S. L., 2003, *The Handbook of Microturbine Generators*, PennWell Corp., Tulsa, OK.
7. Gillette, S., 2010, "Microturbine Technology Matures," Power **154**(11), pp.52-53.
8. McDonald, C. F. and Wilson, D. G., 1996, "The Ultilization of Recuperated and Regenerated Engine Cycles for High-Efficiency Gas Turbines in the 21st Century," Applied Thermal Engineering, 16, pp.635-653.
9. Omatete, O., Maziasz, P. J., Pint, B. A. and Stinton, D. P., 2000, "Recuperators for Advanced Microturbines," Report No. ORNL/TM-2000/304, Oak Ridge National Laboratory, Oak Ridge, TN.
10. Kesseli, J., Wolf, T., Nash, J. and Freedman, S., 2003, "Micro, Industrial, and Advanced Gas Turbines Employing Recuperators," ASME Paper #GT2003-38938, presented at the International Gas Turbine & Aeroengine Congress & Exhibition, Atlanta, GA, June 2-5, 2003.
11. Pint, B. A. and Rakowski, J. M., 2000, "Effect of Water Vapor on the Oxidation Resistance of Stainless Steels," NACE Paper 00-259, Houston, TX, presented at NACE Corrosion 2000, Orlando, FL, March 2000.
12. Asteman, H., Svensson, J.-E., Norell, M. and Johansson, L.-G., 2000, "Influence of Water Vapor and Flow Rate on the High-Temperature Oxidation of 304L; Effect of Chromium Oxide Hydroxide Evaporation," Oxidation of Metals, **54**, pp.11-26.

13. Opila, E. J., 2004, “Volatility of Common Protective Oxides in High-Temperature Water Vapor: Current Understanding and Unanswered Questions,” Materials Science Forum, **461-464**, pp.765-74.
14. Pint, B. A., 2005, “The Effect of Water Vapor on Cr Depletion in Advanced Recuperator Alloys,” ASME Paper #GT2005-68495, presented at the International Gas Turbine & Aeroengine Congress & Exhibition, Reno-Tahoe, NV, June 6-9, 2005.
15. Young, D. J. and Pint, B. A., 2006, “Chromium Volatilization Rates from Cr_2O_3 Scales Into Flowing Gases Containing Water Vapor,” Oxidation of Metals, **66**, pp.137-153.
16. Pint, B. A., 2006, "Stainless Steels with Improved Oxidation Resistance for Recuperators," Journal of Engineering for Gas Turbines & Power, **128**, pp.370-376.
17. Matthews, W. J., More, K. L. and Walker, L. R., 2007, “Accelerated Oxidation of Type 347 Stainless Steel Primary Surface Recuperators Operating Above 650°C,” ASME Paper #GT2007-27916, presented at the International Gas Turbine & Aeroengine Congress & Exhibition, Montreal, Canada, May 14-17, 2007.
18. Pint, B. A., More, K. L., Trejo, R. and Lara-Curzio, E., 2008 “Comparison of Recuperator Alloy Degradation in Laboratory and Engine Testing," Journal of Engineering for Gas Turbines & Power, **130** (1), Art. No. 012101.
19. Rakowski, J. M., Stinner, C. P., Lipschutz, M. and Montague, J. P., “Metallic Alloys for Primary Surface Recuperators,” ASME Paper #GT2006-90680, presented at the International Gas Turbine & Aeroengine Congress & Exhibition, Barcelona, Spain, May 8-11, 2006.
20. Matthews, W. J., More, K. L. and Walker, L. R., (2009) “Comparison of Three Microturbine Primary Surface Recuperators,” ASME Paper #GT2009-59041, presented at the International Gas Turbine & Aeroengine Congress & Exhibition, Orlando, FL, June, 8-12, 2009.
21. Bender, M. D. and Klug, R. C., 2014, “Comparison of Ni-Based 625 Alloy and ATI 20-25+Nb™ Stainless Steel Foils After Long-Term Exposure to Gas Turbine Engine Exhaust,” ASME Paper #GT2014-25334, presented at the International Gas Turbine & Aeroengine Congress & Exhibition, Düsseldorf, Germany, June 16–20, 2014.
22. Pint, B. A., Dryepondt, S., Rouaix-Vande Put, A. and Zhang, Y. 2012, “Mechanistic-Based Lifetime

Predictions for High Temperature Alloys and Coatings," JOM, **64**, pp.1454-1460.

23. Pint, B. A., Unocic, K. A. and Dryepondt, S., 2010, "Oxidation of Superalloys in Extreme Environments," in E. Ott, et al., eds., 7th International Symposium on Superalloy 718 and Derivatives, TMS, Warrendale, PA, pp.861-875.
24. Yamamoto, Y., Brady, M. P., Lu, Z. P., Maziasz, P. J., Liu, C. T. Pint, B. A., More, K. L., Meyer, H. M. and Payzant, E. A., 2007, "Creep-Resistant, Al_2O_3-Forming Austenitic Stainless Steels," Science, **316**, pp.433-436.
25. Pint, B. A., Shingledecker, J. P., Brady, M. P. and Maziasz, P. J., 2007, "Alumina-Forming Austenitic Alloys for Advanced Recuperators," ASME Paper #GT2007-27916, presented at the International Gas Turbine & Aeroengine Congress & Exhibition, Montreal, Canada, May 14-17, 2007.
26. Brady, M. P., Yamamoto, Y., Santella, M. L., Maziasz, P. J., Pint, B. A., Liu, C. T., Lu, Z. P. and Bei, H., 2008, "The Development of Alumina-Forming Austenitic Stainless Steels for High-Temperature Structural Use," JOM, **60** (7), pp.12-18.
27. Pint, B. A., Brady, M. P., Yamamoto, Y., Santella, M. L., Maziasz, P. J. and Matthews, W. J., 2011, "Evaluation of Alumina-Forming Austenitic Foil for Advanced Recuperators," Journal of Engineering for Gas Turbines and Power, **133**, 102302.
28. Pint, B. A., Brady, M. P., Yamamoto, Y., Unocic, K. A. and Matthews, W. J., 2011, "Evaluation of Commercial Alumina-Forming Austenitic Foil for Advanced Recuperators," ASME Paper #GT2011-46704, presented at the International Gas Turbine & Aeroengine Congress & Exhibition, Vancouver, Canada, June, 6-10, 2011.
29. Yamamoto, Y., Brady, M. P., Santella, M.L., Bei, H., Maziasz, P. J. and Pint, B. A., 2011, "Alloy Design Concept for High-Temperature Creep Resistance of Alumina-Forming Austenitic Stainless Steels," Metallurgical and Materials Transactions A, **42**, pp.922-931.
30. Pint, B. A., Dryepondt, S., Brady, M. P., Yamamoto, Y., 2013, "Evaluation of Commercial and Next Generation Alumina-Forming Austenitic Foil for Advanced Recuperators," ASME Paper #GT2013-94940, presented at the International Gas Turbine & Aeroengine Congress & Exhibition, San Antonio, TX, June, 3-7, 2013.

31. Yamamoto, Y., Santella, M. L., Brady, M. P., Bei, H. and Maziasz, P. J., 2009, "Effect of Alloying Additions on Phase Equilibria and Creep Resistance of Alumina-Forming Austenitic Stainless Steels," Metallurgical and Materials Transactions A, **40**, pp.1868-1880.

FIGURE CAPTIONS

Figure 1. Measured Cr depletion from 100μm alloy 625 foil specimens as a function of exposure temperature in wet air for 6-10kh [23].

Figure 2. Light microscopy of polished cross-sections of AFA F4 (a,c,e,g) 80 μm and (b,d,f,h) 106 μm foil specimens after 10,000 h in wet air at (a,b) 650°C, (c,d) 700°C, (e,f) 750°C and (g,h) 800°C.

Figure 3. Summary of creep rupture life and time to 5% strain at 677°C (1250°F)/117MPa and 750°C (1380°F)/100MPa for several commercial alloy foils.

Figure 4. Folded, crushed and welded AFA F4 80μm foil air cell that was assembled into a C65 recuperator.

Figure 5. Sections of the recuperator removed for analysis.

Figure 6. Light microscopy of polished cross-sections of the 80μm F4 foil exposed for 3,000h in a C65 microturbine recuperator. (a) and (b) show a thin surface oxide with occasional small oxide nodules, while (c) shows large oxide nodules observed in one location.

Figure 7. Light microscopy of polished cross-sections of the 80μm alloy 120 foil exposed for 3,000h in a C65 microturbine recuperator. Occasional oxide nodules were observed as shown in (c).

Figure 8. Specimen mass change for new laboratory AFA foils (~100μm thick) compared to commercial AFA F4 foil during 100 h cycles in humid air at 700°C.

Figure 9. Specimen mass change for new laboratory AFA foils (~100μm thick) compared to commercial AFA F4 foil during 100 h cycles in humid air at 800°C.

Figure 10. Summary of creep rupture life and time to 5% strain at 650°C/250MPa and 750°C/100MPa for new laboratory AFA ~100μm foils compared to commercial 106μm F4 foil.

Table 1. Alloy chemical composition (weight %) and average alloy grain size (μm) of the candidate materials.

Alloy	Cr	Ni	Al	Si	Nb	Other	Grain Size (μm)
Type 347	17.8	9.9	0.01	0.5	0.5	1.6Mn	5
709	20.3	24.7	0.05	0.4	0.2	1.5Mo,1.0Mn	16
310	24.1	19.5	0.01	0.3	0.01	1.7Mn,0.2V	10
120	24.7	37.6	0.1	0.2	0.6	0.3Mo,0.7Mn	23-28
625	23.1	63.8	0.2	0.2	0.2	8.9Mo,3Fe	12
AFA*:							
F4 (lab.)	14.0	25.0	3.6	0.1	2.5	2Mn,1W,2Mo,0.1C	45
F4 (comm.)	13.9	25.2	3.5	0.2	2.5	2Mn,1W,2Mo,0.1C	27
F20W (lab.)	13.8	20.1	3.1	0.1	1.0	2Mn,1W,2Mo,0.2C	<10
F20N (lab.)	14.0	20.1	2.9	0.1	1.0	1.9Mn,2Mo,0.2C	<10
F25W (lab.)	13.9	25.3	3.0	0.1	1.0	2Mn,1W,2Mo,0.1C	<10
F25N (lab.)	14.1	25.0	2.9	0.1	1.0	1.9Mn,2Mo,0.2C	<10

* all AFA compositions also contain 0.5Cu and 0.01B

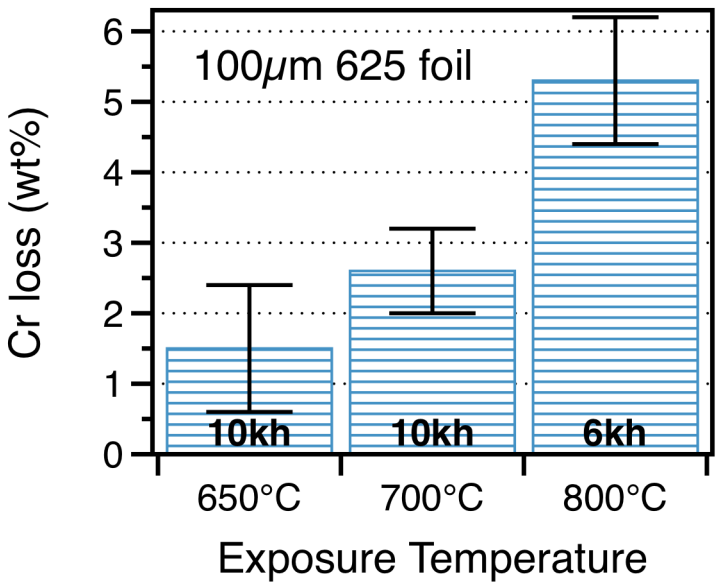

Figure 1. Measured Cr depletion from 100μm alloy 625 foil specimens as a function of exposure temperature in wet air for 6-10kh [23].

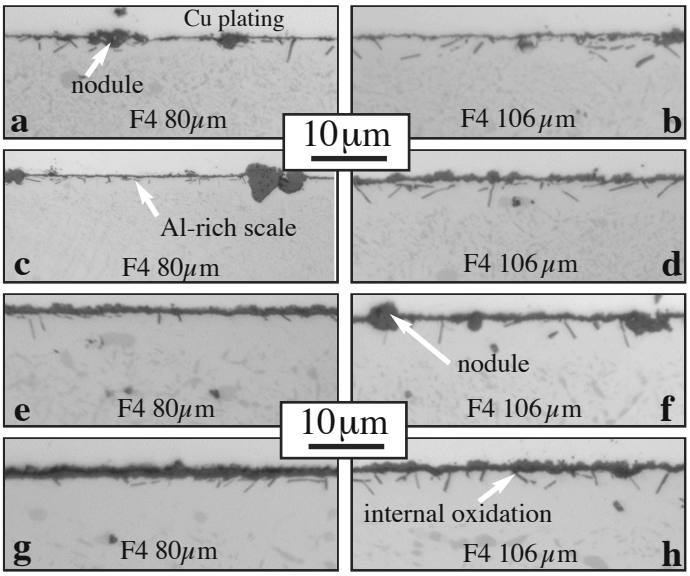

Figure 2. Light microscopy of polished cross-sections of AFA F4 (a,c,e,g) 80 μm and (b,d,f,h) 106 μm foil specimens after 10,000 h in wet air at (a,b) 650°C, (c,d) 700°C, (e,f) 750°C and (g,h) 800°C.

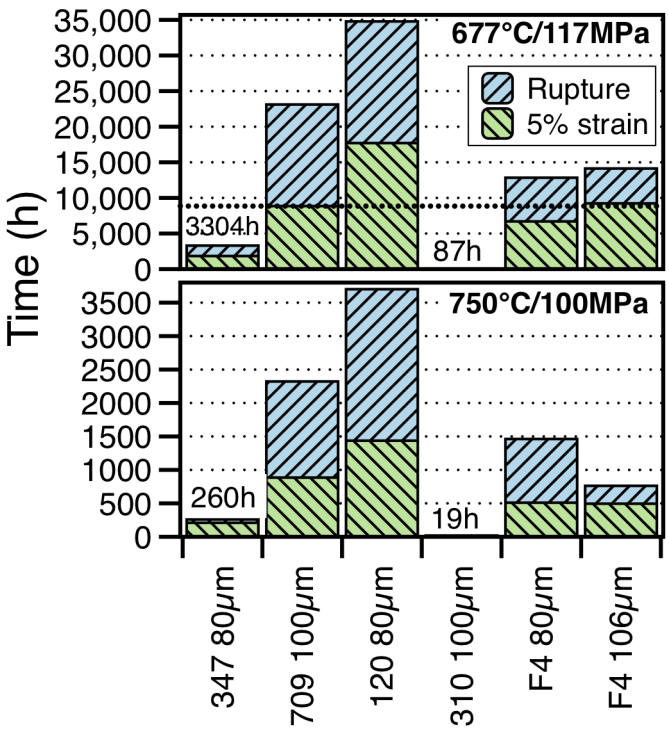

Figure 3. Summary of creep rupture life and time to 5% strain at 677°C (1250°F)/117MPa and 750°C (1380°F)/100MPa for several commercial alloy foils.

Figure 4. Folded, crushed and welded AFA F4 80μm foil air cell that was assembled into a C65 recuperator.

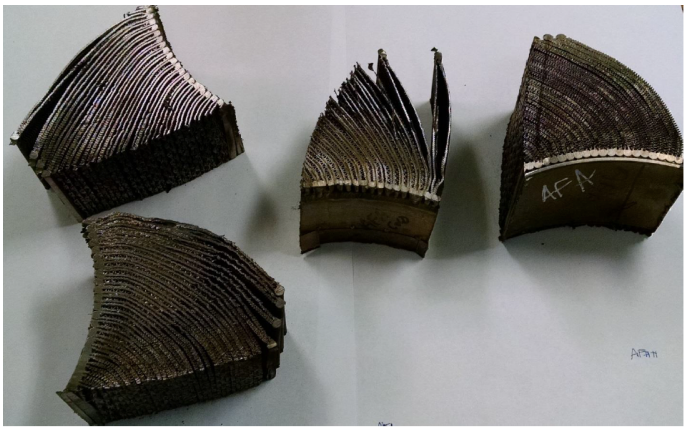

Figure 5. Sections of the recuperator removed for analysis.

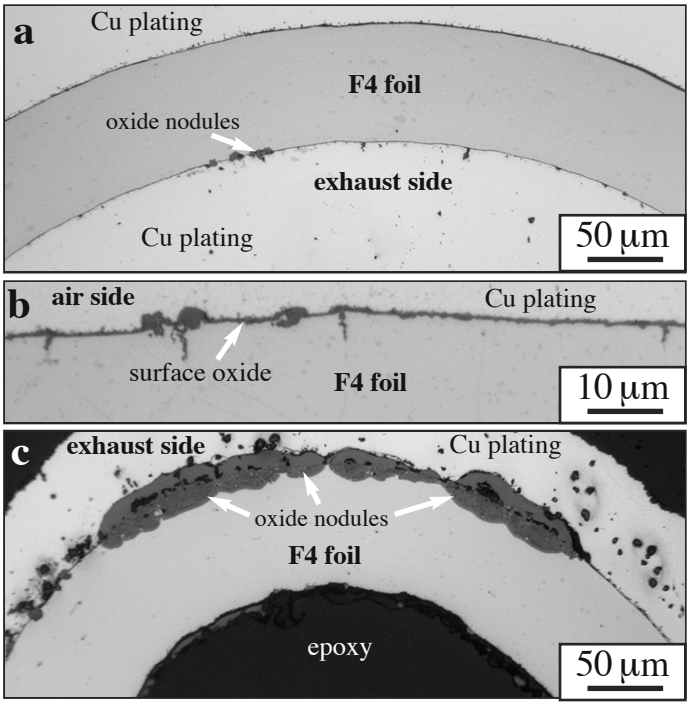

Figure 6. Light microscopy of polished cross-sections of the 80μm F4 foil exposed for 3,000h in a C65 microturbine recuperator. (a) and (b) show a thin surface oxide with occasional small oxide nodules, while (c) shows large oxide nodules observed in one location.

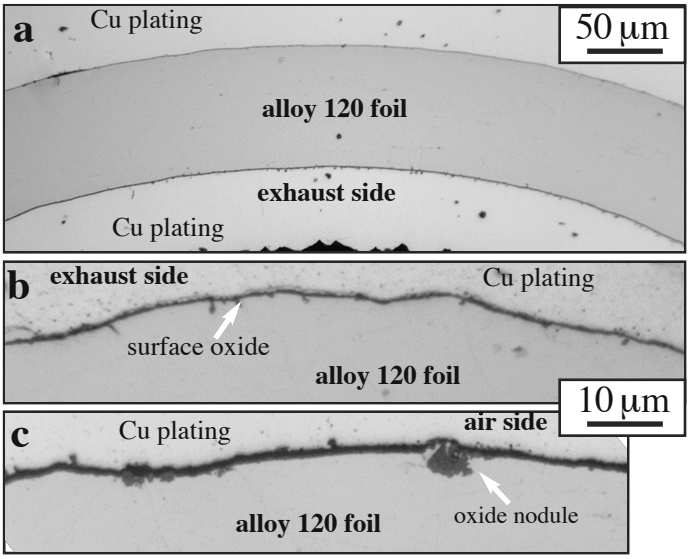

Figure 7. Light microscopy of polished cross-sections of the 80μm alloy 120 foil exposed for 3,000h in a C65 microturbine recuperator. Occasional oxide nodules were observed as shown in (c).

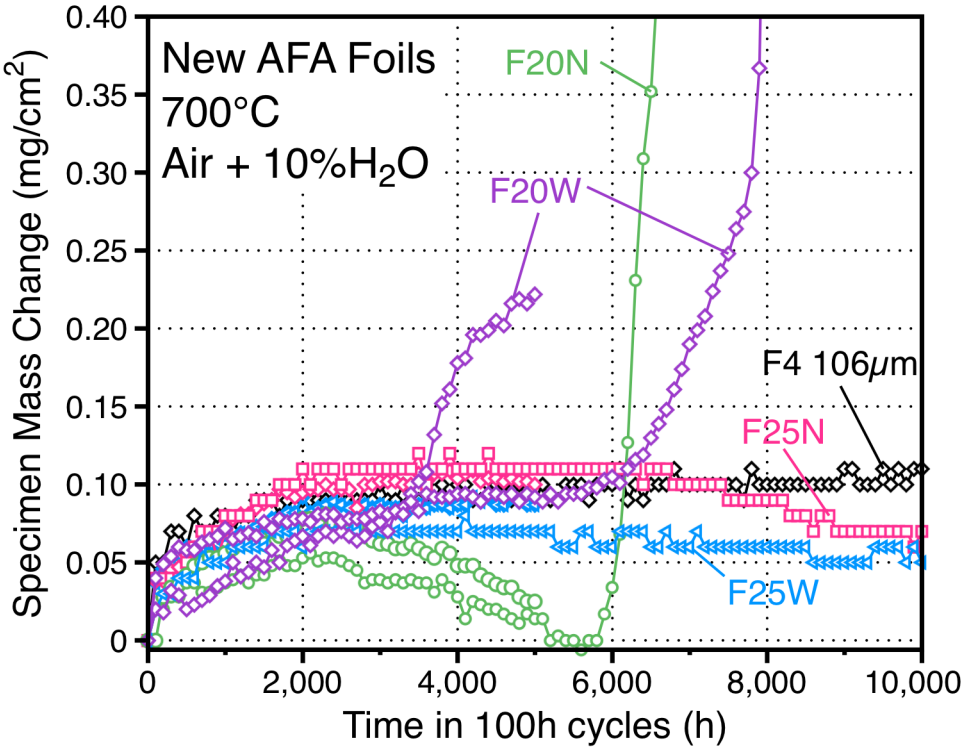

Figure 8. Specimen mass change for new laboratory AFA foils (~100μm thick) compared to commercial AFA F4 foil during 100 h cycles in humid air at 700°C.

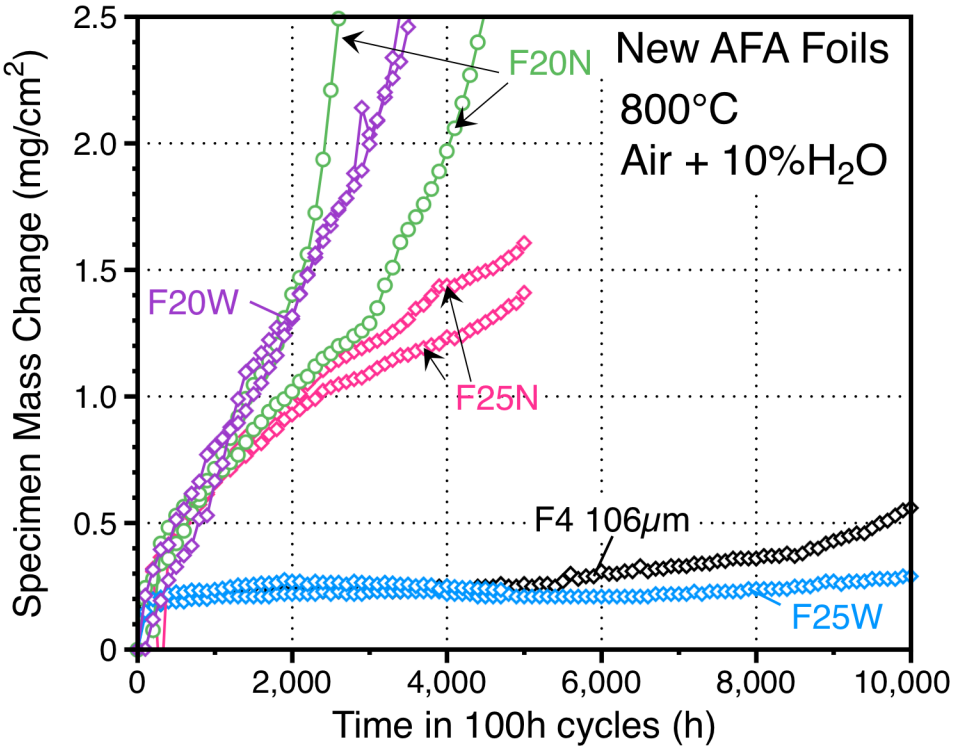

Figure 9. Specimen mass change for new laboratory AFA foils (~100μm thick) compared to commercial AFA F4 foil during 100 h cycles in humid air at 800°C.

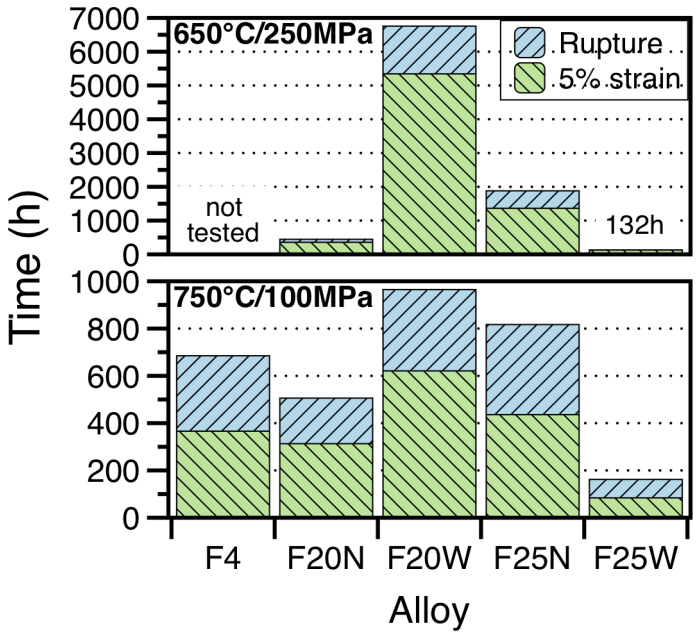

Figure 10. Summary of creep rupture life and time to 5% strain at 650°C/250MPa and 750°C/100MPa for new laboratory AFA ~100μm foils compared to commercial 106μm F4 foil.